Temperature control of open-cathode PEM fuel cells

Stephan Strahl * Ramon Costa-Castelló **

* Institut de Robòtica i Informàtica Industrial (UPC/CSIC), C/Llorens
i Artigas 4, 08028 Barcelona, Spain. Email: strahl.stephan@gmail.com.
** Departament of Automatic Control, Universitat Politècnica de
Catalunya, Barcelona, Spain. Email: ramon.costa@upc.edu

Abstract: Proper temperature control of Proton Exchange Membrane Fuel Cells is a crucial factor for optimizing fuel cell performance. This paper describes a model-based characterization of the equilibrium points of an open-cathode fuel cell system. Phase plane analysis of the nonlinear model versus a linearized model around different points of operation shows the potential of approximating the nonlinear system behavior with a linear model. The system analysis finally serves for the development of a control scheme using robust control techniques. The controller is validated in simulation with the nonlinear plant model.

Keywords: PEM fuel cells, Temperature control, Robust control

1. INTRODUCTION

The industrialized society largely depends on energy that is currently obtained mainly from fossil fuels. Energy demand and carbon emissions have increased over the past 40 years. In addition to the harmful environmental impact, the main concern in this context is the decline of the main fossil fuel sources. This situation has sparked great interest in alternative sources of sustainable energy. In the past two decades different energy sources have emerged, highlighted among them are photovoltaic and wind power. Different studies of the *association of European Renewable Energy Research Centres* (EUREC) in the context of the Seventh Framework Programme for Research and Development have shown that these renewable energy sources have the potential to meet our current energy demand.

Unlike fossil fuels these new sustainable energy sources do not come with implicit storage mechanisms and present the problem of availability linked to appropriate environmental conditions. It is therefore important to achieve efficient energy storage in order to improve energy availability and facilitate transport. An energy carrier that complies with these requirements is hydrogen, which can be produced by all forms of renewable energy. Furthermore, it has significant advantages compared to other energy storage mediums, such as various kinds of batteries, compressed air, or pumped hydro. These are for instance the possibility of long-term energy storage, long distance transport via pipelines with minimal flow resistance, light weight and high energy density. However, topics such as hydrogen storage, infrastructure and low cost production are still challenges that have to be overcome.

Fuel cells are used to convert the stored chemical energy of hydrogen directly into electricity and heat with very high efficiency. Over the past 20 years fuel cells have made significant progress in terms of materials, component design, production cost and energy density of the system. Among the different types of fuel cells, one of the commercially most successful for transportation and portable devices is the PEM (Proton Exchange Membrane) fuel cell (Today, February 2012). This type of fuel cell operates at relatively low temperatures (60^oC-80^oC), which greatly reduces the cost of materials. In addition to low temperature PEM fuel cells show a short startup time, fast transient response, high efficiency and high energy density. In terms of The disadvantages of PEM fuel cells are the still existing durability challenges and a relatively high cost due to the use of platinum as electro-chemical catalyst.

The proton exchange membrane and the ionomer in the porous catalyst layers of this type of fuel cell require the presence of a certain quantity of water in order to guarantee good protonic conductivity. The operation temperature of PEM fuel cells has a strong effect on the water content in the ionomer of the membrane and catalyst layers. Both, the diffusion of water through the membrane as well as the dynamics of water absorption of the ionomer are functions of the temperature (Strahl et al., 2011, 2014b; Majsztrik et al., 2007). The effects of temperature on water transport in the catalyst layers are based on absorption and desorption of water in the ionomer and evaporation and condensation in the pores. As analyzed by means of steady-state modeling, the water content in the catalyst layer has a direct effect on the electrochemically active area (Wang et al., 2004). If water is drained from the pores of the catalyst layer, the amount of protons that reach the active sites for the electrochemical reaction together with the reactant gases and electrons decreases, which in turn decreases the fuel cell's performance. Hence, the optimal management of the temperature and humidity is crucial in PEM fuel cells. Unfortunately it is still not fully understood how to properly control the temperature and humidity of a fuel cell system and its relationship to system efficiency. This paper presents a dynamic model based on the system's temperature and humidity characteristics and the relation to the generated system power. Furthermore,
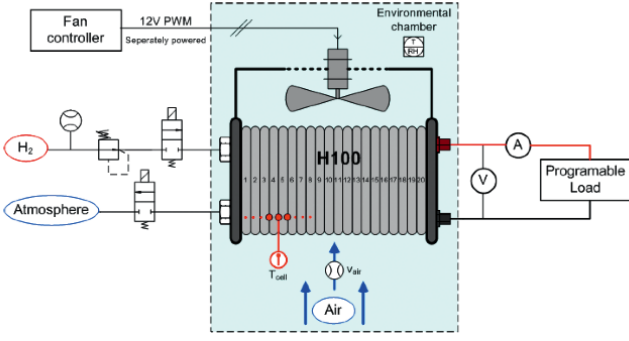
Figure 1. Schematic of the fuel cell system H-100 installed in laboratory test station

the dynamic system behavior is characterized and a robust temperature controller is proposed.

2. SYSTEM DESCRIPTION

In this study the commercial PEM fuel cell stack H-100 developed by *Horizon Fuel Cells Technologies* is analyzed. This stack is composed of 20 cells and has a rated power of 100W. This stack has an open-cathode and does not require reactant gas humidification. It is air cooled and has an active area of 22.5cm^2. It includes a single cooling fan directly attached to the housing of the fuel cell. Stack cooling is achieved by forced convection through the cathode flow channels, while providing oxygen to the cathode at the same time. Therefore, the cathode air supply and the fuel cell cooling cannot be decoupled.

Figure 1 shows a schematic diagram of the fuel cell system installed in the laboratory test station. The fan is powered by a $12\,\text{V}$ external power source. A controller sets the rotational speed of the fan by adjusting the PWM duty cycle. The air speed is measured using a high precision airflow sensor *E75 E + E Elektronik*. The anode inlet is fed with dry hydrogen. A manual pressure regulator keeps the pressure of the anode inlet constant at about $0.4\,\text{bar}$.

3. SYSTEM MODELING

In a previous work Strahl et al. (2014a) a dynamic second-order model has been developed for the system described in the section 2. The model is defined by the following set of equations:

$$\dot{T}_{fc} = K_1 \cdot I_{fc}V_{fc} + K_1 \cdot I_{fc}^2$$
$$\qquad + \left(K_2 \cdot T_{amb} - K_2 \cdot T_{fc}\right) u \qquad (1)$$
$$\dot{s}_{fc} = K_3 \cdot T_{fc} - K_4 \cdot f_p\left(T_{fc}\right) \cdot s_{fc} - f_d\left(s_{fc}\right) \qquad (2)$$
$$V_{fc} = K_5 \cdot T_{fc} \cdot f_a\left(T_{fc}, s_{fc}, I_{fc}\right) \qquad (3)$$

The dynamic states correspond to the fuel cell temperature (T_{fc}) and liquid water saturation (s_{fc}). The latter represents to the ratio of the volume of liquid water to the total volume of empty space in the porous structure of the catalyst layer (Pasaogullari and Wang, 2004). The system has 3 inputs which are the fuel cell current (I_{fc}), the ambient temperature (T_{amb}) and the cathode inlet air

velocity (u). The latter is often used as control action. The output of the system, V_{fc}, corresponds to the fuel cell stack voltage. Thus, the generated electrical power by the stack is defined by $V_{fc} \cdot I_{fc}$.

The equations (1)-(3) are highly nonlinear, because of the involved complex expressions f_p, f_d and f_a composed by nonlinear components Strahl et al. (2014a). In addition, the control action is multiplied by functions that depend on the dynamic states.
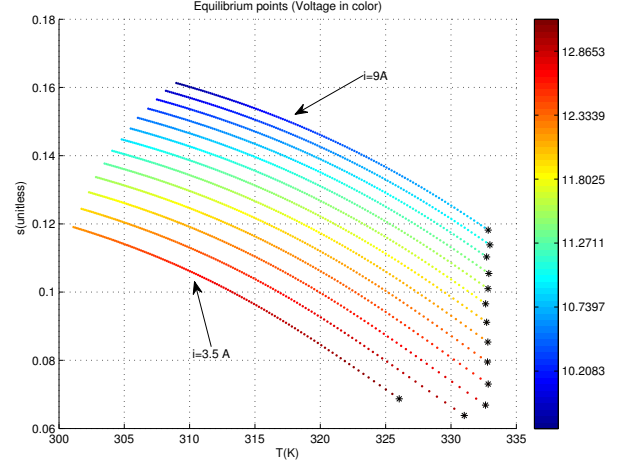
4. EQUILIBRIUM POINT CHARACTERIZATION

Figure 2. Equilibrium points for different values of the stack current.

In order to characterize the system's operating points, the equilibrium points of (1)-(3) are analyzed. The analysis is simplified by the following variable change:

$$u \triangleq \frac{v}{K_2 T_{amb} - K_2 T_{fc}} \qquad (4)$$

where v corresponds to the heat extracted from the system. With this variable change, the system description results in:

$$\dot{T}_{fc} = K_1 \cdot I_{fc} \cdot V_{fc} + K_1 \cdot I_{fc}^2 + v \qquad (5)$$
$$\dot{s}_{fc} = K_3 \cdot I_{fc} - K_4 \cdot f_p\left(T_{fc}\right) \cdot s_{fc} - f_d\left(s_{fc}\right) \qquad (6)$$
$$V_{fc} = K_5 \cdot T_{fc} \cdot f_a\left(T_{fc}, s_{fc}, I_{fc}\right) \qquad (7)$$

As the equations are highly nonlinear, it is not possible to perform an analytic analysis of the equilibrium points. Alternatively a numerical procedure is applied. The equilibrium points can be obtained by equating $\dot{T}_{fc}$ and $\dot{s}_{fc}$ to zero in equations (5) and (6), and sweeping the two exogenous inputs (I_{fc},v). The ranges of the different variables are selected in a way to cover the experimentally characterized operating range of the system: The ambient temperature, T_{amb}, is usually is in the range of $[278, 308]$K, the load current, I_{fc} can be adjusted in the range of $[0, 8]$A, the air velocity set by the fan u, is within the range of $[0.1, 1]$m/s, the liquid water saturation, s_{fc}, moves within the range $[0.01, 0.8]$ and finally the fuel cell temperature is usually in the of $[T_{amb}, 333]$K. Figure 2 shows the equilibrium points obtained for different values of the stack current.
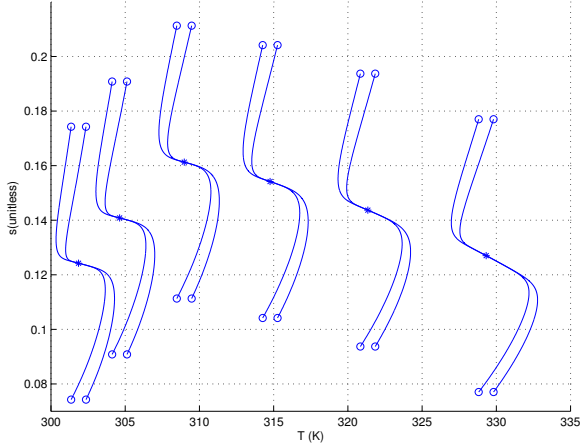
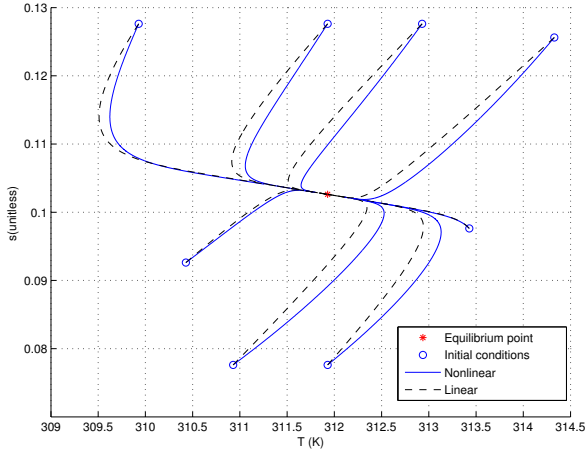Figure 3. Phase plane plot for different operating points.

Figure 5. Step response of different linear models obtained around different equilibrium points.

Figure 4. Comparison of the linearized model with the nonlinear model.
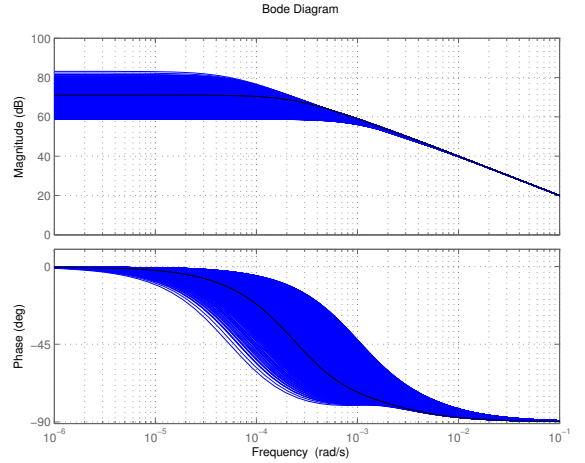
Figure 6. Bode diagram of the different linear models obtained around different equilibrium points.

Within this analysis a relationship between the liquid water saturation, fuel cell temperature and current has been established, which can be used to calculate the equilibrium points of s:

$$s_{fc}^* \approx \alpha_{00} + \alpha_{10}T_{fc}^* + \alpha_{01}I_{fc}^* + \alpha_{11}T_{fc}^*I_{fc}^* + \alpha_{02}(I_{fc}^*)^2 \quad (8)$$

where $\alpha_{00} = 0.714$, $\alpha_{10} = -0.002108$, $\alpha_{01} = 0.00411$, $\alpha_{11} = 4.063e - 05$ and $\alpha_{02} = -0.0006086$.

Additionally, it is possible to obtain the value of the control action (v) for a given temperature and current:

$$v^* \approx \beta_{00} + \beta_{10}T_{fc}^* + \beta_{01}I_{fc}^* + \beta_{11}I_{fc}^*T_{fc}^* + \beta_{02}I_{fc}^2 \quad (9)$$

where $\beta_{00} = 0.0326$, $\beta_{10} = -9.593e - 05$, $\beta_{01} = -0.06164$, $\beta_{11} = 0.0001137$, $\beta_{02} - 0.0009065$. This relationship can be used as a *feedforward term* in the control system.

5. DYNAMIC BEHAVIOUR

A numerical analysis has been applied to analyze the dynamic behavior of the system defined by equations equations (5)-(6). Although showing high complexity, the system's order is low, which allows for a graphical analysis
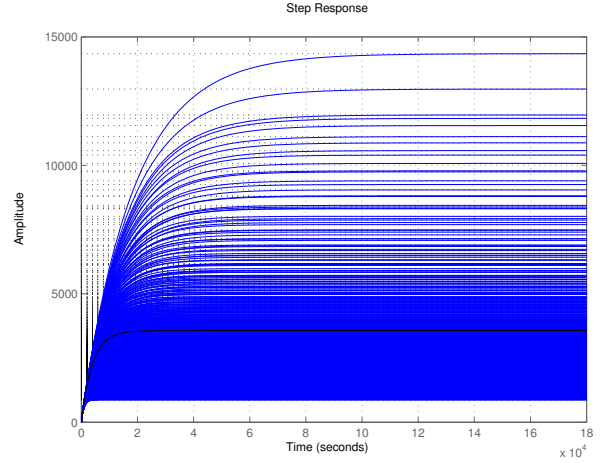
of the phase plane. Figure 3 shows the evolution of the system around several equilibrium points for constant values of v and I_{fc}. As it can be observed, the states' behavior is stable and quite similar for all the depicted situations. The system trajectories resemble those of a linear system with two real poles in the left half-plane (Khalil, 2002).

Figure 4 shows the trajectories of the nonlinear system defined by equations (5)-(6) in the phase plane, compared with the trajectories of a linear system for different initial conditions, keeping v and I_{fc} constant. The linear system representation is obtained via linearization around one equilibrium point (Khalil, 2002). As it can be seen, both trajectories are quite similar, which indicates that despite the system's complexity, as analyzed in (Strahl et al., 2014a), the system can be easily approximated by a linear system.
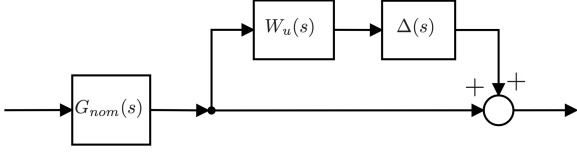
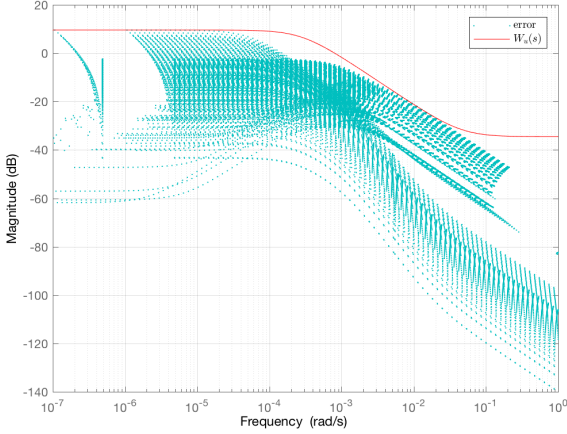Figure 7. Block diagram of the linear system with multiplicative uncertainty.

Figure 8. Uncertainty magnitude weighting function, $W_u(s)$ and relative error of the different transfer functions from the nominal one.
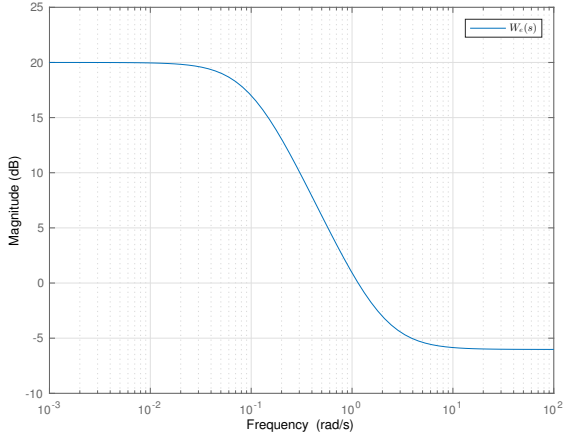

Figure 9. Sensitivity weighting function, $W_e(s)$, frequency response.

6. CONTROLLER DESIGN

The previous section demonstrated that the nonlinear system defined by equations (5)-(6) can be described by a linear system with a similar dynamic behavior in all characterized equilibrium points. Hence, it seems reasonable to assume that a single linear controller can be applied for proper temperature control of the system. Thus, the frequency response and step response obtained from linear models around different equilibrium points, shown in Figure 2, are analyzed. Figure 5 shows the step response

of different linear models. It can be seen that despite being second order systems, their step response is very similar to that of a first order system. However, although the shape is similar, there is a significant variation in gain and time constant between the different systems, which in the frequency domain leads to the differences in cut-off frequency and phase, shown in Figure 6.

In order to model this variability, a numerical analysis using the MATLAB command ucover (Balas et al., 2012) has been performed. Firstly, a nominal model has been selected:

$$G_{nom}(s) = \frac{s + 0.001567}{(s + 0.001794)(s + 0.0002448)}. \quad (10)$$

Secondly, the relative error of a relevant number of transfer functions, corresponding to different equilibrium points, with respect to the nominal transfer function is computed. A boundary of the error at each frequency is calculated, which is used to obtain the transfer function, $W_u(s)$:

$$W_u(s) = \frac{0.00016194(s + 5.631)}{s + 0.0003025}. \quad (11)$$

In this case a first order system is good enough, shown in Figure 8. Combining the nominal plant, $G_{nom}(s)$ and the uncertainty multiplicative function, $W_u(s)$, a generalized plant is defined (Figure 7).

Once this model is obtained, it seems natural to use a performance specification based on an error weighting function and a subsequent performance adjustment by H_∞ or μ-synthesis (Sánchez-Peña and Sznaier, 1998). The chosen performance specifications for the weighing function is:

$$W_e(s) = \frac{0.01(s + 100)}{s + 0.1}. \quad (12)$$

The magnitude of $W_e(s)$ is shown in Figure 9. This specification ensures a tracking error smaller than 10% within the desired bandwidth (0.1rad/s) and excellent robustness margin.

Analyzing Figure 8 and Figure 9 it can be seen that both the uncertainty and the performance weighting functions present high gain at lower frequencies. This is contradictory from the point of view of the formulation of the control problem, hence a direct solution using either H_∞ or μ-synthesis (Sánchez-Peña and Sznaier, 1998) will hardly generate satisfactory results.

Gain uncertainty in the low frequency range is unlikely to cause instability since the phase around those frequencies is close to zero. This type of reasoning can not be applied to a model with unstructured uncertainty. Consequently, the unstructured uncertainty model depicted in Figure 8 is replaced by a structured uncertainty model (Sánchez-Peña and Sznaier, 1998) defined as:

$$W'_u(s) = \frac{k}{\tau s + 1} \quad (13)$$

where $k \in [1, 3.16]$ and $\tau \in [0.000455, 0.00105]$. The uncertainty parameters have been obtained by analyzing Figures 6 and 8. This kind of uncertainty can easily be considered in a process of μ-synthesis.

In order to ensure zero steady-state error in following steps of the controller design, an integrator is added in series with the plant. Later on, this integration will become part of the designed controller.
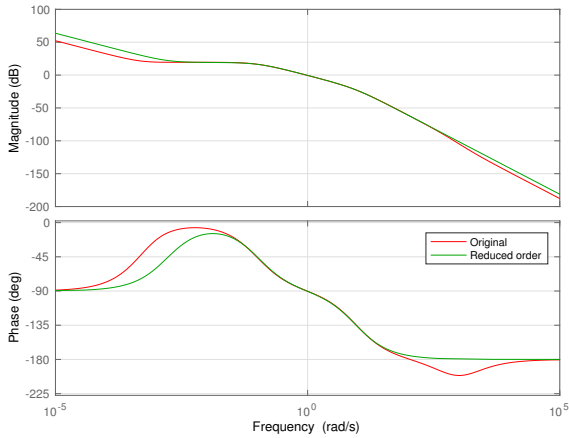
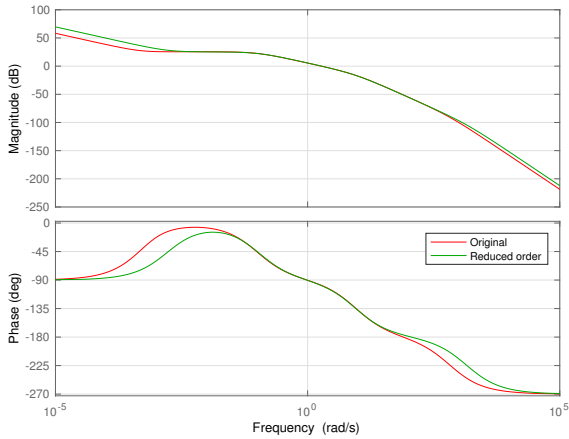Figure 10. Frequency response of both, the original full order and the reduced order controller.

Figure 11. Open-loop nominal system frequency response for the original full order and the reduced order controller.
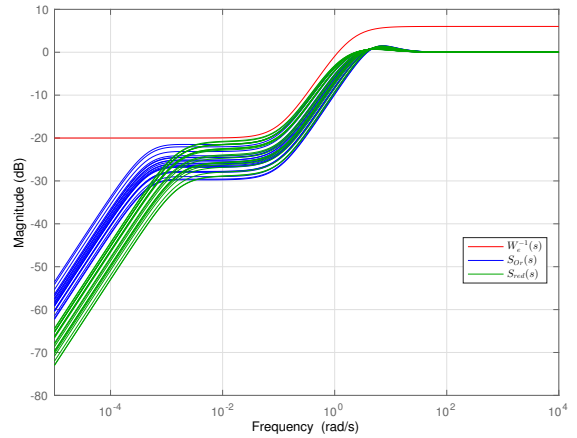

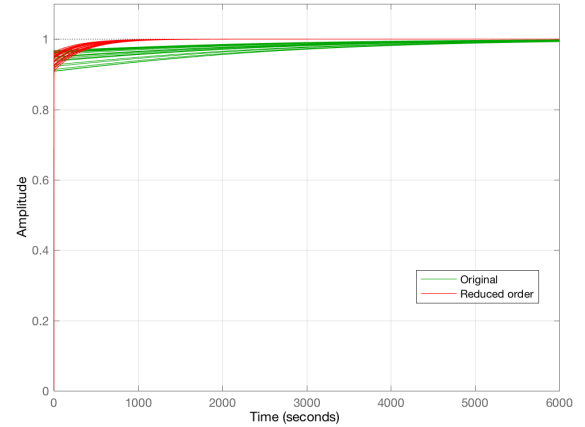Figure 12. Sensitivity of the closed-loop system.

Figure 13. Closed-loop system step response for different transfer functions corresponding to different equilibrium points for full and reduced order.

The controller is designed in MATLAB using the *Robust Control Toolbox* (Balas et al., 2012). The μ-synthesis procedure generated a 7th order controller. In order to obtain a simpler controller an order reduction method has been applied. A second order controller, that presents a good approximation of the original controller has been obtained. Using the robuststab command from the *Robust Control Toolbox* (Balas et al., 2012), it has been confirmed that both controllers generate a robustly stable system, providing the desired performance.

Figure 10 shows the frequency response of the original controller and reduced order controller. The reduced order controller presents higher gain in the low frequency range, which is a desirable characteristic, but it also shows higher gain in the high frequency range, which in principle is an undesired characteristic (however, not that relevant in this application because the plant is shows a low pass frequency response). But despite this, the overall gain is small and therefore no amplification of measurement noise

is introduced. Figure 11 shows the frequency response of the open-loop nominal system. The gain component is quite similar while the phase differs slightly in the middle frequencies. However, the phase remains within reasonable intervals in both cases.

Finally, Figure 12 shows the sensitivity function obtained for a number of possible plants, for both the original and the reduced order controller. It is shown, that for both cases all sensitivity functions are below the bounds imposed by $W_e^{-1}(s)$, consequently the system will show robust performance. Figure 13 shows the step response of the complementary sensitivity functions of both controllers and different possible plants. All closed-systems evolve similarly, with a similar error, time constant and no overshoot.

As a consequence, a small order controller that provides robust performance has been chosen for application in the control scheme.
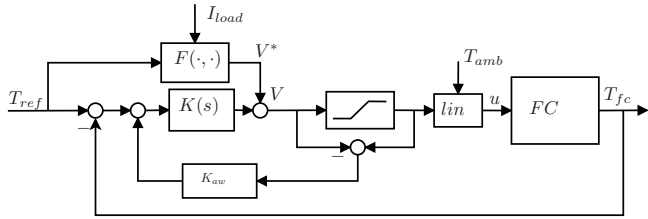
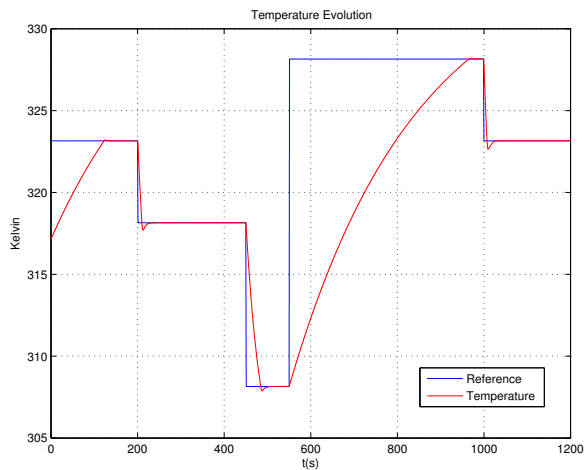Figure 14. Complete schematic of the controlled system.

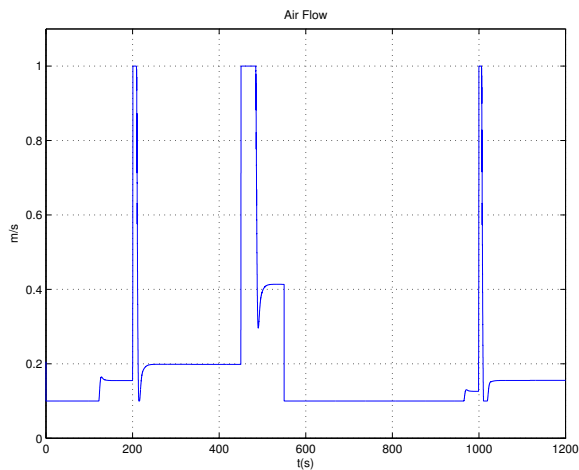Figure 15. Closed-loop temperature time response using with the nonlinear model.

Figure 16. Closed-loop system control action time response time response using with the nonlinear model.

7. CONTROLLER VALIDATION

The proposed controller is composed of the partial linearization introduced in equation (4), the linear controller, $K(s)$, obtained in the previous section, and a feedforward element, $F(\cdot, \cdot)$ based on equation (9). This term is responsible for setting the values in the ideal stationary values. Finally, an antiwindup scheme is introduced for managing the control action saturation.

For implementation purposes, the controller has been discretized with a sampling period of 0.01 s.

Figure 15 shows the evolution of the closed-loop system using the nonlinear plant model (section 3). In the simulations a constant load current of 4 A and a constant ambient temperature of 298 K were set. All restrictions of the real system have been taken into account. The control system perfectly follows the reference temperature with a slight overshoot. Figure 16 shows the respective control action, which indicates the limited cooling capacity by the maximum air flow limit and also the limited stack heating dynamic by the minimum air flow required for providing oxygen. The applied antiwindup scheme works properly, hence the control action quickly returns to the proper range after saturation.

8. CONCLUSIONS

This work presents the design of a control system for temperature control of an open-cathode PEM fuel cell stack. The developed methodology is not limited to this specific type of fuel cells as it takes into account the nonlinear nature of the system and generates a controller with a simple structure and good closed-loop behavior. Currently, the authors are working on the experimental validation of the control system.

REFERENCES

Balas, G., Chiang, R., Packard, A., and Safonov, M. (2012). *Robust Control Toolbox. User's Guide. R2012a.* Mathworks.

Khalil, H.K. (2002). *Nonlinear Systems.* Prentice Hall, Upper Saddle River, New Jersey, 3. edition edition.

Majsztrik, P.W., Satterfield, M.B., Bocarsly, A.B., and Benziger, J.B. (2007). Water sorption, desorption and transport in nafion membranes. *Journal of Membrane Science*, 301(1–2), 93 – 106. doi: 10.1016/j.memsci.2007.06.022.

Pasaogullari, U. and Wang, C. (2004). Liquid water transport in gas diffusion layer of polymer electrolyte fuel cells. *Journal of the Electrochemical Society*, 151(3), A399–A406.

Sánchez-Peña, R.S. and Sznaier, M. (1998). *Robust Systems Theory and Applications.* Adaptive and Learning Systems for Signal Processing, Communications and Control Series. Wiley-Interscience.

Strahl, S., Husar, A., Puleston, P., and Riera, J. (2014a). Performance improvement by temperature control of an open-cathode pem fuel cell system. *Fuel Cells*, 1–3. doi: 10.1002/fuce.201300211.

Strahl, S., Husar, A., and Franco, A.A. (2014b). Electrode structure effects on the performance of open-cathode proton exchange membrane fuel cells: A multiscale modeling approach. *International Journal of Hydrogen Energy*, 39(18), 9752 – 9767. doi: 10.1016/j.ijhydene.2014.03.218.

Strahl, S., Husar, A., and Serra, M. (2011). Development and experimental validation of a dynamic thermal and water distribution model of an open cathode proton exchange membrane fuel cell. *Journal of Power Sources*, 196(9), 4251 – 4263. doi:10.1016/j.jpowsour.2010.10.074.

Today, F.C. (February 2012). The fuel cell today industry review 2011. *http://www.fuelcelltoday.com/analysis/industry-review/2011/the-industry-review-2011.*

Wang, Q., Eikerling, M., Song, D., and Liu, Z. (2004). Structure and performance of different types of agglomerates in cathode catalyst layers of pem fuel cells. *Journal of Electroanalytical Chemistry*, 573(1), 61 – 69. doi:10.1016/j.jelechem.2004.06.022.